Computational Fluid Dynamics Modelling and Analysis of Heat Transfer in Multichannel Dimple Plate Heat Exchanger

P. Soman, Divya
Department of Chemical Engineering, School of Engineering, Cochin University of Science and Technology, Kochi, Kerala, INDIA

Karthika, S.
Department of Chemical Engineering, Vellore Institute of Technology, Vellore, Tamil Nadu, INDIA

Valan, D.T.; Kalaichelvi P. *+, Radhakrishnan T.K.
Department of Chemical Engineering, National Institute of Technology, Tiruchirappalli, Tamil Nadu, INDIA

ABSTRACT: *In the present study, Computational Fluid Dynamics is used for heat transfer studies in the dimple, and flat plate heat exchangers. By employing water as a working medium (fluid), the same and different flow analyses were numerically studied. SOLID WORKS 2018 software was used for the study. The study primarily investigated the effect of the flow rate of hot fluid on the overall heat transfer coefficient. The study also analyzed the influence of hot fluid's Reynolds number on cold fluid's Nusselt number. It was observed that an increase in the mass flow rate of the hot fluid from 0.016 to 0.067 kg/s resulted in an increase in the heat transfer coefficient from 65 to 298 W/(m^2.K) for* the *dimple plate heat exchanger (DPHE). Meanwhile, an increase in the Reynolds number of the hot fluid (from 200 to 1000), induced an increase in the Nusselt number of the cold fluid from 1.9 to 8.7 for DPHE. A correlation was developed to calculate the Nusselt number for the same flow analysis of the flat plate heat exchanger (FPHE). The study also compared the performance of the DPHE with that of the FPHE. The results of the same flow analysis indicated that the DPHE exhibited a Nusselt number value 39% greater than the FPHE at the highest mass flow rate of 0.067 kg/s, while in different flow analysis, the DPHE demonstrated a Nusselt number value 41% greater than the FPHE at the highest mass flow rate of 0.067 kg/s.*

KEYWORDS: *Plate heat exchanger; Computational fluid dynamics; Flow analysis; Nusselt number; Overall heat transfer coefficient.*

INTRODUCTION

Computational Fluid Dynamics (CFD) is a science that visualizes and elucidates problems concerning fluid flow, heat, and mass transfer employing computational algorithms. The use of high-speed supercomputers for CFD studies not only reduces the time of simulations in solving highly complicated and large problems but also aids in achieving

***** *To whom correspondence should be addressed.*
+ *E-mail: kalai@nitt.edu*
1021-9986/2022/6/2071-2086 16/$/6.06

better solutions. These simulations are performed by specifying the surfaces with boundary conditions. CFD is widely applied in many fields such as aerodynamics, weather simulation, design and analysis of industrial systems, marine engineering, *etc.*[1]. The knowledge of fluid dynamics, numeric, and modeling helps in designing the geometric domain for solving real-time problems. The application of CFD in the design of Heat Exchangers (HEs) gives an insightful prediction of how fluid behaves and the dynamics of heat and mass transfer in a control volume. With the aid of CFD, the performance of the HE can be enhanced by controlling the parameters *viz.* feed temperature, feed pressure, shell dimensions, tube quantity, tube configuration, baffle spacing, *etc.* The performance of the HE is also influenced by the surface geometry of the heat transfer area. The heat transfer augmentation studies by amending the surface (existing) of the HE is a very interesting research area. Surface roughness techniques like protrusions, dimples, and twisted tapes are some of the heat transfer augmentation techniques applied to HE. *Luki* and *Ganesan* [2] observed that the use of dimples in the inner tube of double-pipe HE displayed 8% better effectiveness than smooth double-pipe HE. Alumina nanofluid (outer tube) as the working fluid and hot flue gas (inner tube) were employed. *Saleh* and *Abdel-Hameed* [3] analyzed the performance of a dimple plate in a parallel-flow HE with two channels using water as a working fluid. A FLUENT computation package with k-ε turbulence model was employed for the numerical studies [3]. The GAMBIT code was used for developing the geometry and mesh. It was observed that the dimple-surfaced HE showed better efficiency than normal smooth-surfaced HE. The enhancement in heat transfer coefficient was 250% with a pressure drop of 150 to 200% compared to smooth PHE.

Oluyale et al. [4] experimentally investigated the effect of dimple arrangement on airflow and heat transfer characteristics in a single channel/rectangular duct. For their study, three plates with even, uneven arrangement of dimple plates and smooth plates was employed. The results of the study indicated that unevenly and evenly arranged dimple plate channels had 91.8% and 75.7% increase in Nusselt number (Nu) over the smooth channel. In both the dimple arrangements (uneven and even), there was less than 1% increase in the friction factor when compared to the smooth channel. *Zhang et al.* [5] numerically investigated the heat transfer and flow characteristics in a cross-combined dimple tube with k-ε turbulence model. Air was considered as the working medium. It was observed that the heat transfer enhancement rises by 18.8 – 48.3 % and an average of 24.8% when compared with the traditional single ellipsoidal tube. *Lofti* and *Sunden* [6] performed numerical simulation studies to study the influence of five kinds of concave dimple turbulators (elliptical dimple, trapezoidal prism dimple, conical frustum dimple, upward triangular dimple, and leeward triangular dimple) on thermo-hydraulic performance enhancement in a plate fine-and elliptical tube heat exchanger. ANSYS CFX was the computational package used for the study. The shear stress transport k-ω turbulence model was used for numerical modeling. High resolution is the discretization scheme used. The dimples were modeled on the fin surface transversely between the elliptical tubes. The study revealed that the upward triangular dimple had better performance among the different dimple turbulators investigated due to its special structural shape in both upstream and downstream regions.

Firoozi, *Majidi*, and *Ameri* [7] numerically studied the heat transfer performance and flow characteristics in dimple tubes with water and Al_2O_3/water as the working fluids. The investigation primarily focused on finding a superior configuration of the dimpled tube (by varying dimple height, dimple pitch, and dimple filling angle) with water as the working medium. Then, Al_2O_3/water was used as the working fluid to study the effect of the addition of nanoparticles in the base fluid. Nanoparticle volume fractions varied from 1 to 4%. The finite volume method was adopted for the numerical study [7]. The shear stress transport k-ω turbulence model was used for numerical modeling. The semi-Implicit Method for Pressure-Linked Equations (SIMPLE) algorithm was used for pressure-velocity coupling. Second order upwind scheme was used for the discretization of convection and diffusion terms. The results indicated that the overall performance of the dimpled tube increased with a decrease in dimple pitch, an increase in dimple height, and an increased filling angle. Furthermore, maximum thermal-hydraulic performance was obtained at Re= 2000 with 4% nanofluid in the optimum dimpled tube configuration (dimple filling angle= 120^0, dimple height = 2.00 mm, and dimple pitch = one dimple diameter) [7]. *Sabir et al.* [8] also performed numerical studies on dimpled tubes with conical, spherical, and ellipsoidal dimples. Reynolds Average

Navier Stokes (RANS) model was used for the steady state conditions and large eddy simulations for unsteady conditions. ANSYS Fluent was the computational package used. Pressure velocity coupling was solved by pressure-based coupled algorithms, gradients in diffusion terms were solved by the least square cell-based method, and pressure gradient was approximated by a second-order interpolation scheme while second-order upwind scheme for momentum and energy. *Babu* and *Sellamuthu* [9] performed numerical simulations to investigate the heat transfer and fluid flow characteristics in a concentric dimpled tube double-pipe heat exchanger with a parallel flow arrangement. Water was used as the working medium. The geometry of the model was developed with SOLID WORKS software and further steps of the study were performed using ANSYS. The pressure velocity coupling was done using SIMPLE algorithm, discretization method adopted was second-order upwind. The k-ε turbulence model was the model employed for the study [9]. *Piper et al.* [10] performed numerical studies on a pillow-plate heat exchanger. In this study, the pillow plate is modified by adding dimples to the pillow plates. The results indicated that the new structured surface of the pillow plates promoted stronger near-wall mixing. The CFD simulations were solved using STAR-CCM+ (Siemens AG) solver based on the finite volume method. The flow field was described by the Reynolds-Averages-Navier-Stokes (RANS) equations. Reynold's stress was determined using the elliptical blending k-ε model.

Yoon et al. [11] demonstrated direct numerical simulation studies of a cooling channel with six different configurations with one common dimple and five different (tear-drop) dimples by altering the dimensions of the upstream cavity of the dimple. The work studied the effect of heat transfer and flow characteristics of air at a Reynolds number (Re) of 2800 and a Prandtl number (Pr) of 0.71. It was observed that the tear-drop dimples displayed better performance than the general dimple. The tear-drop dimple with 1.3 upstream dimensionless lengths of the cavity exhibited +4% better volume goodness factor ratio than the general dimple. A numerical study of laminar airflow was performed by *Shokouhmand, Esmaeili,* and *Vahidkhah* [12] in a parallel-plate dimpled channel (single channel) with dimples located on both walls. FLUENT computation package was used for the numerical model. The discretization of the convective and diffusive fluxes was modeled using the QUICK scheme. The pressure-velocity coupling was handled with the SIMPLE method. Results indicated that an increase in the number of dimples increases the value of Nu. It was also observed that a decrease in the relative depth of the dimple increased heat transfer. The study indicated that an optimum relative depth for the dimple is essential to obtain a higher value of Nu and heat flux. In the study, the dimple cavity with a relative depth of 0.2 was observed as an optimum value. *Ligrani et al.* [13] experimentally investigated the change in the local Nu and flow structure in a passage with projections and dimples on opposite walls. It was found that in walls with a protrusion, an improvement in the value of the local Nu and friction factor was witnessed. It was also observed that the value of Nu was enhanced close to the downstream edges of the dimples, indicating that heat transfer augmentation is possible with protrusion and dimples on the opposite walls of the rectangular channel.

Chimres, Wang, and *Wongwises* [14] studied fin and tube HE with the semi-dimple arrangement. 135 different configurations of the fin with semi-dimples were evaluated via the numerical method by the commercial software 'ANSYS CFX 17.0'. The shear stress transport k-ω turbulence model was used for numerical modeling. It was observed that the semi-dimple arrangement exhibited a goodness factor in the range of 33–37%, which was higher than the existing arrangement. It was found that the goodness factor was 15–20% higher than the plain fin. *Vorayos et al.* [15] experimentally examined the heat transfer analysis of the external flow of air over 14 different types of dimple plates with an inline and staggered arrangement. The study found that the staggered arrangement was offering a 26% higher performance Nusselt number (Nu) than smooth plates, and the inline arrangement was displaying a 25% higher performance than the smooth plate.

From the literature, it can be noted that the heat transfer behavior in dimple channels is affected by the dimple depth [16], alignment [16,17], diameter [18,19], types [17,20,21], and channel height [22]. It can also be observed that the studies on dimples are confined to single- or two-channel plates and tube-type HE. Moreover, most of the studies are based on working fluids such as air and flue gas. In the present study, a CFD analysis was done for a dimple plate HE (DPHE) with more than two channels *viz.* six channels using SOLID WORKS software (2018 version). The same and different flow analyses were performed with water

as both cold and hot working fluids. The CFD model validation was done by comparing the DPHE simulated results with the actual experimental results. Finally, the DPHE and Flat Plate Heat Exchangers (FPHE) were compared to assess the heat transfer performance.

THEORETICAL SECTION

CFD modeling and simulation

The finite volume method is adopted to solve the flow and heat transfer in the PHE. The initial stage in the CFD simulation is the creation of geometry, which was generated employing SOLID WORKS 2018. The software requires certain governing equations that are mentioned elsewhere [23]. It basically solves the Navier-Stokes equations, which are formulations of mass, momentum, and energy conservation laws. The simulation was elucidated employing the standard k-ε turbulence model available in the software [23]. The pressure-velocity coupling was achieved with a SIMPLE algorithm. Second-order upwind was used to discretize diffusion and convection terms.

The requisite geometry was defined by developing the necessary domain of known dimensions (Table 1). The generation of the mesh was done using a trial-and-error method. Fluids that are supposed to be present in the flow geometry were defined. The material properties of the geometry and the boundary conditions were mentioned. The domain was then simulated in the SOLID WORKS flow simulation software to solve all the governing equations numerically. The post-processing, the final stage in CFD, was performed to filter the simulation data to visualize the contour plots. A total of 2 hours was required for the completion of one simulation run. The temperature of the outlet and the temperature distribution of the fluids between the channels were recorded during all simulation runs. It was assumed that cold, as well as hot fluids, were flowing through three channels counter currently. Two simulation analyses – same and different flow analyses – were conducted in FPHE and DPHE with water as hot and cold side working fluid.

Defining the geometry

The geometry of the FPHE and DPHE was created using the SOLID WORKS 2018 software. Firstly, the geometry of a single flat plate, single dimple plate (dimple depth of 0.003 m and dimple diameter of 0.005 m), inlet, and outlet ports were generated using the 'Part' section of the software. Later, using the assembly option of the software, the parts were assembled to generate the FPHE and DPHE as shown in Figs. 1 and 2, respectively. The dimensions of the PHEs are given in Table 1. Fig. 3 clearly shows the arrangement of dimples and the single dimple plate used in the CFD analysis for DPHE domain generation.

Table 1: Dimension of the PHEs.

Specification	Value
Plate length, L	0.425 m
Plate width, W	0.125 m
Plate thickness, t	0.0008 m
Channel width, S	0.004 m
Number of pass	Single
Number of channels	6
Thickness of gasket	0.004 m
Number of plates, N_P	7

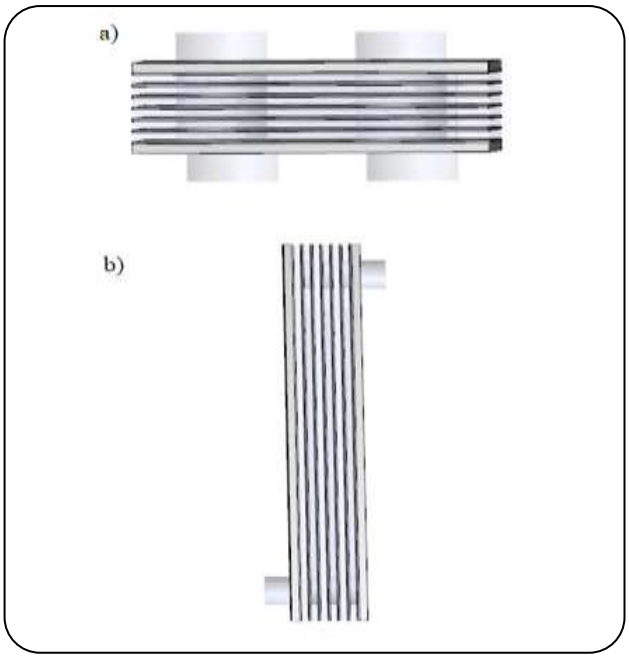

Fig. 1: Geometry of FPHE a) Top view b) Side view.

Mesh generation

The meshing of the geometric domain was generated using SOLID WORKS 2018 version software, and the heat, mass, and momentum equations were solved.

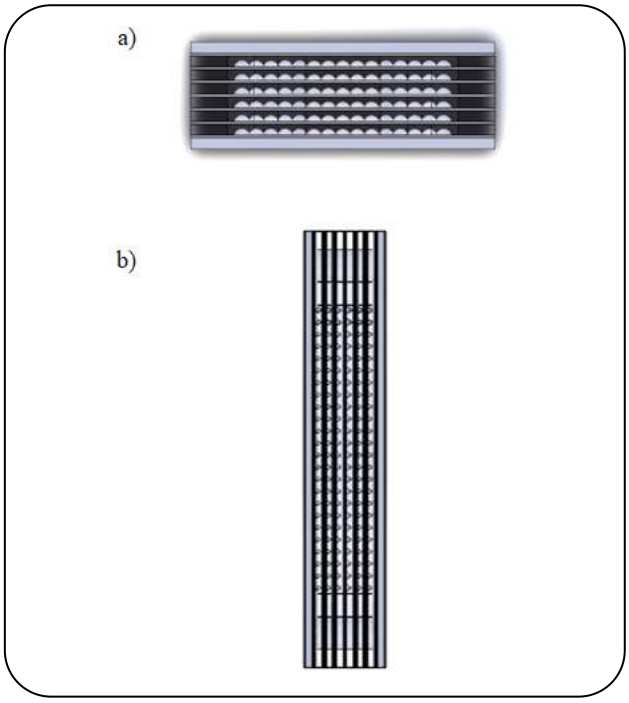

Fig. 2: Geometry of DPHE a) Top view b) Side view.

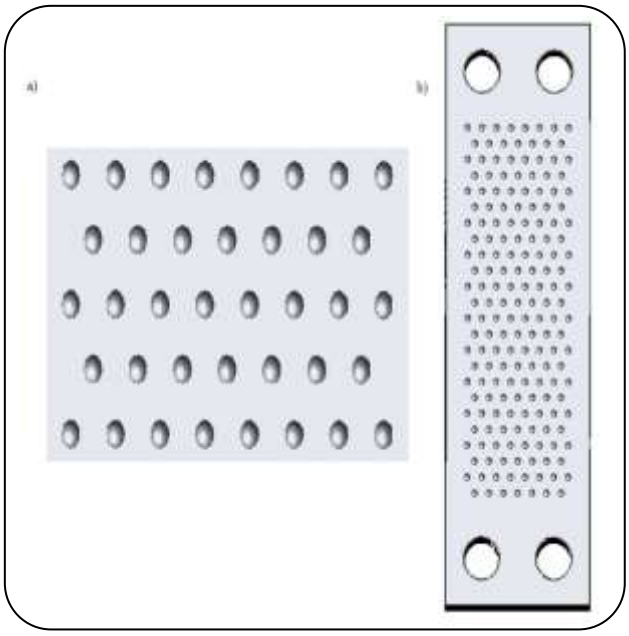

Fig. 3: Dimple geometry a) staggered arrangement b) Dimple plate.

The mesh grid independency test was performed for the six-channeled FPHE and DPHE. A total of 10,62,802 tetrahedral cell elements were obtained as the optimum mesh for the two exchangers. Tetrahedral meshing with 0.3-mm spacing was applied for the plate volumes and the fluid channels.

Specifying material properties and boundary conditions

The next step in CFD simulation was the specification of boundary conditions. The boundary conditions of the hot and cold fluid inlets were assigned as mass flow inlets and outlets for both FPHE and DPHE. The metal plates were modeled as thin walls displaying a thermal resistance of 0.0008-m stainless steel. All the exterior walls were modeled as an adiabatic system. The simulations were performed with no-slip conditions at all walls. The geometry was modeled with water as a flowing fluid and the properties of the same were also specified. The fluid flow passing through the FPHE and DPHE was assumed to flow in the counter-current direction, as illustrated in Fig. 4. The simulations were performed for different combinations of hot and cold flow rates varying from 1–4 LPM of hot fluid and 2–4 LPM of cold fluid. The cold fluid inlet temperature was assumed at 303.2 K, while the hot fluid was set at 353.2 K.

Grid Independency Study

Mesh independency test is performed for the six-channeled FPHE and DPHE to reduce the influence of the number of grids on the computational results. The results of the grid independency test are given in Tables 2 and 3. As the number of mesh increases, there is an increase in the simulation time. From Tables 2 and 3, it is clear that when the mesh number increases from 2 to 3 there is a decrease in the % error and when the mesh number increases from 3 to 4 the % error increases. Hence, a total of 10,62,802 tetrahedral cell elements are obtained as the optimum mesh for both exchangers.

Data reduction

In the present simulation study, the hot and cold fluid temperatures at the exit of FPHE and DPHE were obtained from the CFD flow simulation software. The temperature contours were also obtained for various mass flow rates of hot and cold fluid streams. From the temperature of the cold and hot fluid outlets, the bulk means temperatures were acquired, and the thermophysical properties of the fluid streams (hot and cold) were determined. The model equations used for the analysis of heat transfer [24] were used for predicting the overall heat transfer coefficient (U-value) and Nu.

Table 2: Grid Independency Study for DPHE.

Mesh No.	Total Cells	Temperature of Fluid		% Deviation	
		Hot Fluid	Cold Fluid	Hot Fluid	Cold Fluid
Base: 0	7,14,535	342.8	307.1	--	--
1	8,73,256	342.5	307.8	0.088	0.227
2	9,85,256	342.1	308.7	0.117	0.292
3	10,62,802	342.0	309.0	0.029	0.097
4	11,54,709	341.5	309.8	0.146	0.258

Table 3: Grid Independency Study for FPHE.

Mesh No.	Total Cells	Temperature of Fluid		% Deviation	
		Hot Fluid	Cold Fluid	Hot Fluid	Cold Fluid
Base: 0	7,14,535	342.7	304.7	--	--
1	8,73,256	342.4	305.1	0.088	0.131
2	9,85,256	341.4	307.1	0.292	0.651
3	10,62,802	341.3	307.3	0.029	0.065
4	11,54,709	340.7	308.4	0.176	0.357

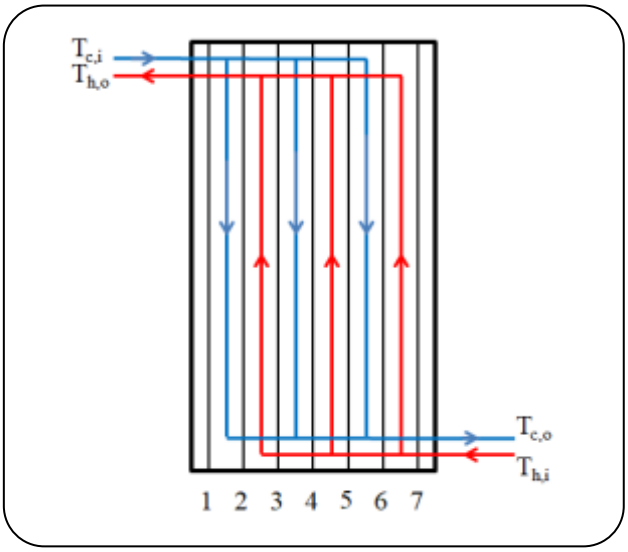

Fig. 4: Flow pattern in PHE.

RESULTS AND DISCUSSION

Validation of the CFD model of DPHE

For validating the CFD model, Nu was obtained from the experiments [24] of the DPHE with water as a working fluid (hot and cold). The Nu value obtained was compared with that calculated from the current simulation study. The experimental setup was similar to the DPHE geometry domain (Fig. 3) with seven dimple plates and six channels, three each for the hot and cold fluid streams. Re_h (Reynolds's number of the hot fluid) varied in the range of 200–1080 for the DPHE experimental study. For the same flow analysis, the Nusselt number of cold fluid (Nu_c) was obtained for the water–water system from the experiment and simulation runs, as presented in Table 4.

From Fig. 5, it is evident that all simulated data for DPHE lie within ± 20% deviation from the experimental data. It should be noted the simulated models took place in perfect adiabatic conditions; however, the experimental systems underwent a heat loss. Hence, a positive difference between the simulated and experimental values was observed.

Correlation for heat transfer analysis of FPHE

Using CFD simulation, the same flow analysis was performed for the FPHE. A correlation was developed using the simulation results of the same flow analysis study. A correlation taking into account Re and Pr was developed to determine the Nu. Eq. (1) was developed using numerical regression and is applied to Re ranging from 200 to 860.

$$Nu_{\square} = 0.006Re^{0.921}\,Pr^{0.33} \quad for 200 < Re < 860 \quad (1)$$

Table 4: Comparison between experimental and numerical results.

Flow rate (LPM)		Nu_c		Percentage error ((Simulation Value – Experimental)/ Experimental) ×100
Cold fluid	Hot fluid	Experimental	Simulation	
1	1	1.25	1.49	19.5
2	2	2.25	2.69	19.14
3	3	3.47	4.16	19.81
4	4	5.72	6.7	17.82

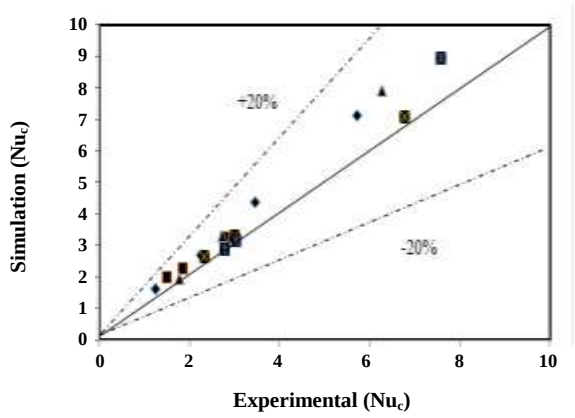

Fig. 5: Validation plot for DPHE.

Where Nu_h is the Nusselt number of the hot fluid, *Re* denotes the Reynolds number, and *Pr* signifies the Prandtl number of the hot fluid [24].

Same flow analysis results

The simulation studies were conducted for the FPHE with the same flow rates of hot and cold fluid streams. The hot, as well as cold fluid flow rates, were simultaneously varied from 0.016 to 0.067 kg/s. The temperature contours of the fluids in the cold and hot channels for various flow rates in the FPHE are shown in Figs. 6 and 7. From Fig. 6 it is evident that when the flow rate of the cold fluid increases, its residence time decreases. This, in turn, leads to a decrease in the outlet temperature of the cold fluid. This can be appreciated by the color changes observed from Fig. 6(a) to Fig. 6(d). In Fig. 6(a), the temperature contour of the fluid in the cold channel is seen as a mixture of light blue, green, and yellow colors. As the flow rate of the cold fluid increases (shown in Figs. 6(b), (c), and (d)), the light blue, green, and yellow color change to dark blue, and dark green with negligible yellow color, respectively. Correspondingly, in Fig. 7, when the flow rate of the hot fluid stream increases, the outlet temperature of the hot fluid increases. This could be due to the short residence time of the hot fluid in the FPHE. This can be seen from the color change observed from Fig. 7(a) to Fig. 7(d). In Fig. 7(a), the temperature contour of fluid in the hot channel is seen as a mixture of dark green, light brown, and light yellow. As the flow rate of hot fluid increases, as shown in Figs. 7(b), (c), (d) the dark green, light brown, and light-yellow change to a less area of light green, a more area of light yellow and dark brown. This indicates higher temperatures of the hot channel output at a higher flow rate (0.067 kg/s).

The same flow analysis was also performed in the DPHE with water. The observed temperature contours are given in Figs. 8 and 9. In Fig. 8, the flow rate of the cold fluid, increases from 0.016-0.067 kg/s, an increase in the cold outlet temperature can be observed from the larger extent of yellow, light green, and light blue colors (Fig. 8(d)). This could be because of the increased residence time (caused due to dimple geometry) when compared with flat plates for the same flow rates. Similarly, in Fig. 9 when the flow rate of the hot fluid increases from 0.016-0.067 kg/s, there is an increase in the outlet temperature of hot fluid which can be witnessed from the larger extent of red, orange, yellow, light green, and a less area of dark green as observed in Fig. 9(d). Hence, from Figs. 8 and 9 it can be inferred that with higher flow rates, higher temperatures can be obtained at cold and hot outlets in the DPHE. Additionally, while comparing the temperature contours of cold channels of the FPHE with DPHE (Figs. 6 and 8), a perceptible mix of light yellow, light green, and blue can be seen in the DPHE compared to darker blue-green shades in the FPHE.

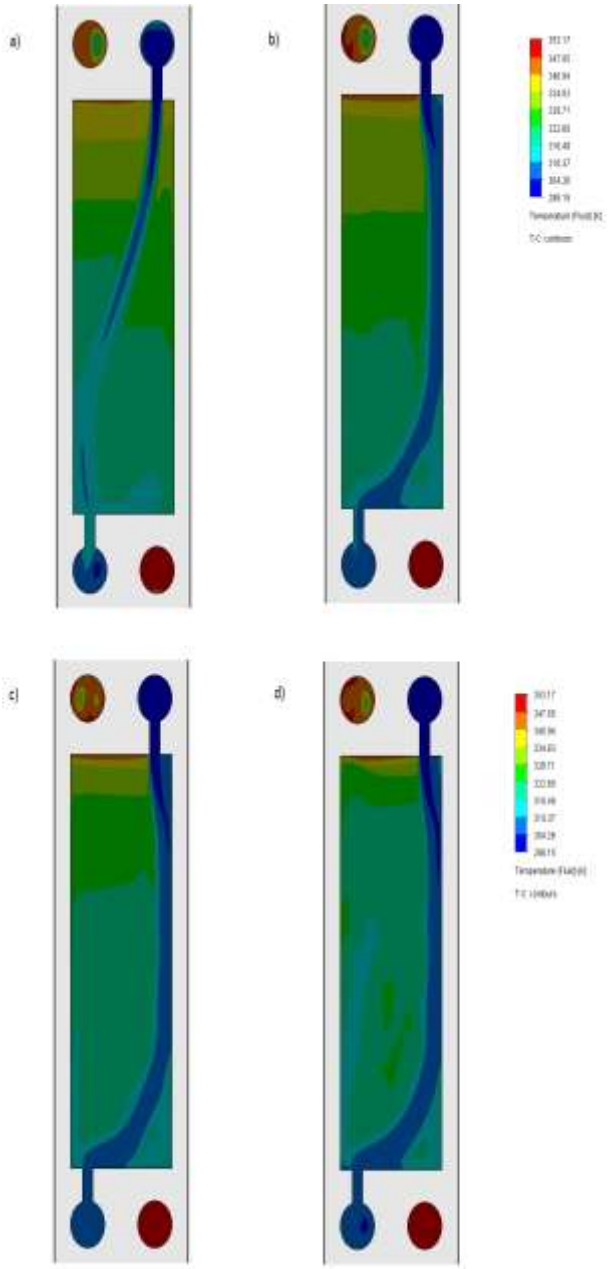

Fig. 6: The temperature contour of the fluid in the cold channel in FPHE with a) 0.016 kg/sb) 0.033 kg/s c) 0.05kg/s d) 0.067 kg/s.

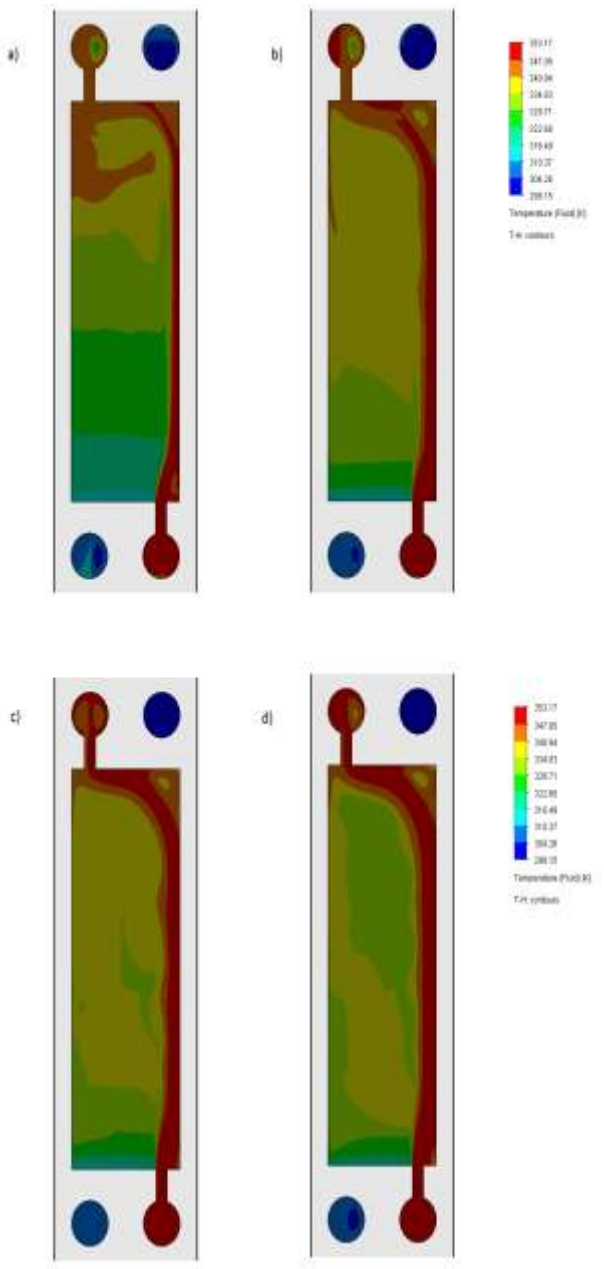

Fig. 7: The temperature contour of the fluid in the hot channel in FPHE with a) 0.016 kg/s b) 0.033 kg/s c) 0.05 kg/s d) 0.067 kg/s.

Similarly, while comparing the hot channel temperature contour of the FPHE with DPHE (Figs. 7 and 9), there is a visible mix of light yellow, light green, orange (outlet), and red (inlet) in the DPHE as compared to mild yellowish-green with a reddish tint and dark reddish-brown in the FPHE. This shows that the hot outlet temperature in the DPHE is lower than that in the FPHE, and the cold outlet temperature is higher in the DPHE than in the FPHE. This is due to the formation of the vortex, which in turn enhances the turbulence of the fluid. The increase in residence time is due to the dimple configuration. *Mahmood et al.* [25] and *Ahmed*, *Qureshi*, and *Qureshi* [26] observed similar vortex formations with dimples on the heat transfer surfaces. Flow visualization studies by *Mahmood et al.* [25] performed on a dimpled surface placed on one wall of a channel show vortical fluid

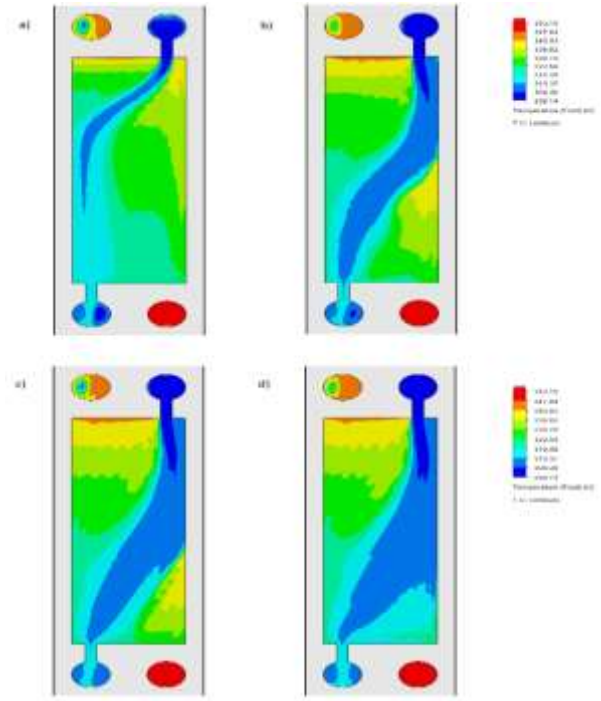

Fig. 8: Temperature contour of the fluid in the cold channel in DPHE with a) 0.016 kg/s. b) 0.033 kg/s c) 0.05 kg/s d) 0.067 kg/s.

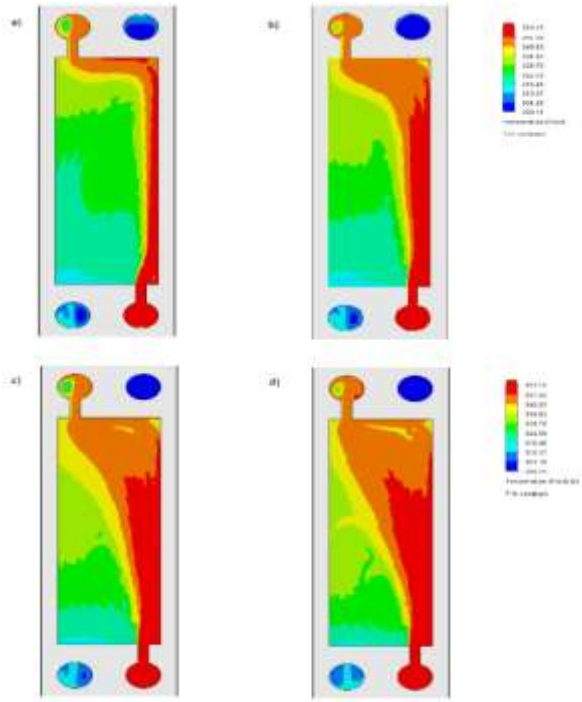

Fig. 9: Temperature contour of the fluid in the hot channel in DPHE with a) 0.016 kg/s. b) 0.033 kg/s c) 0.05 kg/s d) 0.067 kg/s.

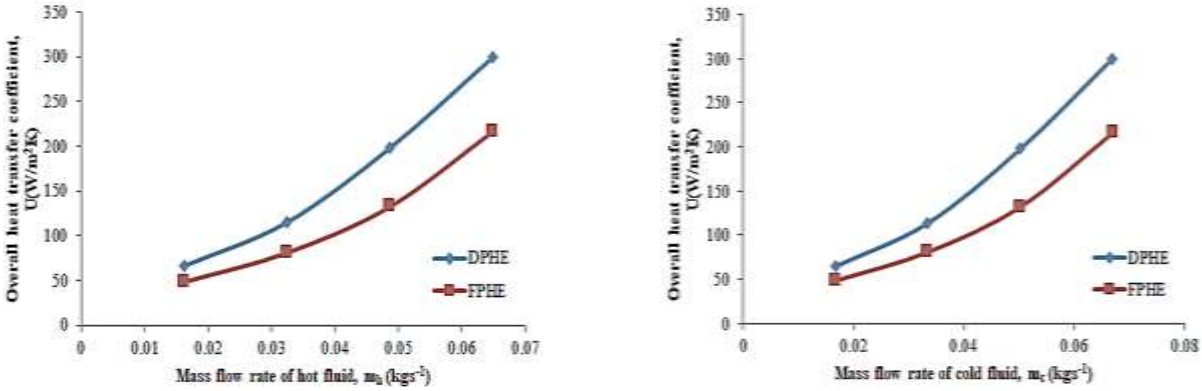

Fig. 10: a) Effect of m_h on U, b) Effect of m_c on U.

and vortex pair shed from the dimples. *Ahmed*, *Qureshi*, and *Qureshi* [26] observed that turbulence and vortex formation is the result of intermixing of a relatively low velocity of mainstream flow and a higher velocity of flow that enters and leaves the dimples in their CFD study of single-sided dimpled PHE.

From the temperature contours obtained for both FPHE and DPHE, the steady-state outlet temperatures of the cold and hot fluid streams are noted. The U-value was calculated, and the results are plotted in Fig. 10 for both FPHE and DPHE.

From Figs. 10 (a) and (b), it can be noted that as the flow rate of the hot and cold fluid streams increases, the U-value increases for both FPHE and DPHE. In the case of FPHE, this is also seen from the temperature contours of Figs. 6 and 7, and for DPHE, this is seen in Figs. 8 and 9. It can be observed from Figs. 10 (a) and (b) that the U-Value of the DPHE is higher than that of FPHE at

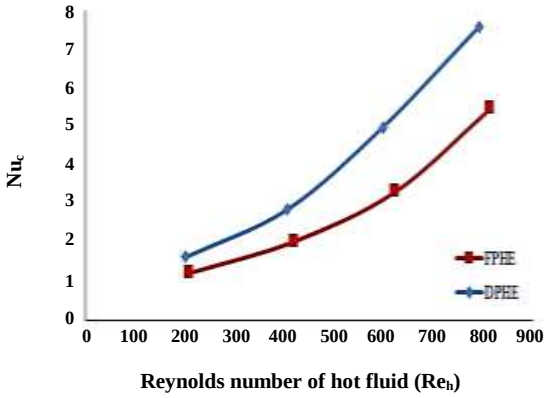

Fig. 11: Effect of Re_h on Nu.

all flow rates (hot fluid 0.016-0.067 kg/sand cold fluid 0.016-0.067 kg/s). When the flow rate of hot and cold fluid streams increases, an increase in the U-value from 33 to 39% in the DPHE was noted. This increase is attributed to the presence of dimples on the plates, which create turbulence in the flow of fluid due to vortex formation. This is also reinforced by the color patterns in Figs. 8 and 9 (DPHE) compared to Figs. 6 and 7 (FPHE).

As the heat transfer coefficient is dependent on several parameters, the dimensionless numbers (Nu, Re, Pr) are utilized to develop empirical correlations taking into account factors such as surface geometry and thermophysical properties of the fluids. Hence, the thermal performance of both FPHE and DPHE was also analyzed in terms of dimensionless numbers *viz.*, Nu and Re.

The steady-state outlet temperatures of cold and hot fluids are noted for both FPHE and DPHE from the same flow simulation. The thermophysical properties estimated at bulk fluid temperature, along with the simulated steady-state temperatures, were used to calculate the dimensionless numbers required for the heat transfer study of both FPHE and DPHE. Fig. 11 shows the influence of Re_h on Nu_c. It can be noted that as Re_h increases, Nu_c of both FPHE and DPHE increases. Also, it can be observed that when the mass flow rate of the fluid increases, Re_h increases. The increase in Re_h results in increased turbulence in the fluid stream leading to an enhancement of Nu_c. In addition, from Fig. 11, it can be inferred that Nu_c of the DPHE is more than that of the FPHE at all flow rates which can be evidenced while comparing Figs. 6 and 7 with Figs. 8 and 9. This is due to the artificial roughness technique such as dimples which induce an increase in the flow pattern of the fluid stream passing through the exchanger channels. It can be noticed that at the highest flow rate of 0.067 kg/s, the DPHE performs 39% more than FPHE. As the fluid propagates through the DPHE, more secondary flow patterns were generated at higher flow rates (Fig. 8(d) and Fig. 9(d)), which leads to an increase in the vortices formed in the dimples, which eventually augment heat transfer.

Different flow analysis results

In general, a different flow analysis is more advantageous than the same flow analysis as the variation in flow rate and temperature profile can be easily identified in the HE designs. Hence, different flow analysis was performed in the present study by varying the flow rates of hot fluid streams from 0.016 to 0.067 kg/s and cold fluid streams from 0.033 to 0.067 kg/s. The results are presented in Fig. 12, and it can be observed that an increase in the mass flow rate of the hot fluid stream resulted in an increase in the U-value of the fluid. This is due to the fact that the amount of heat transferred is directly proportional to the flow rate of the hot fluid stream for a given geometry of the heat transfer equipment. The DPHE performed better than FPHE. It was noted that when the cold fluid flow rate was increased from 0.033 to 0.067 kg/s, the U-value increased from 65 to 298 W/(m^2.K) for DPHE, while the U-value of FPHE varied from 57 to 213 W/(m^2.K).

There was an increase in the U-value when the flow rate of the hot fluid stream was increased, which can be seen in Fig. 12(a), for a cold fluid mass flow rate of 0.033 kg/s. The temperature contours, a result of simulating the FPHE for the same cold fluid stream flow rate (0.033 kg/s) and hot fluid stream flow rate of 0.016 and 0.05 kg/s, are presented in Fig. 13 for both cold and hot channel sides. The changes in temperature contours observed in both hot and cold channels (Fig. 13) validate the results of the U-value in Fig. 12(a). Similarly, the higher U-value for DPHE obtained in Fig. 12(a) is also substantiated while comparing the temperature contours of DPHE presented in Fig. 14 with those of FPHE (Fig. 13) for identical simulation conditions.

Fig. 12(b) illustrates that the U-value increases with an increment in the flow rate of hot fluid stream at a uniform flow rate of cold fluid (0.05 kg/s) for both the FPHE and DPHE. For FPHE, the temperature contours obtained

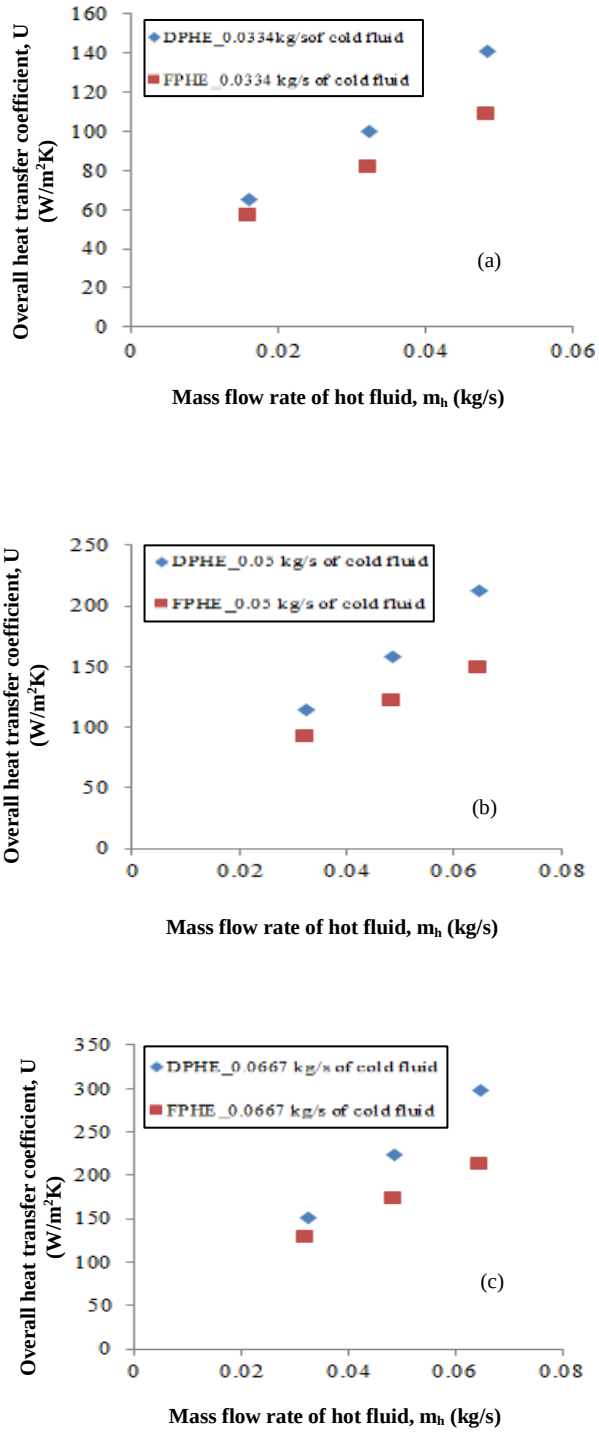

Fig. 12: Effect of m_h on U for different flow analyses.

By setting the cold fluid stream flow rate constant at 0.05 kg/s and changing the hot fluid flow rate to 0.033 kg/s and 0.067 kg/s are shown in Fig. 15. The increment in the U-value of the DPHE (when compared to FPHE) as shown in Fig. 12(b) can be visualized with the color variance of the temperature contours of hot and cold fluid channels of DPHE presented in Fig. 16 for the same operating parameters studied for FPHE (Fig. 15).

Fig. 12(c) shows an increment in U-value at a uniform cold fluid flow rate of 0.067 kg/s with an increase in the hot fluid flow rate. Fig. 17 illustrates the temperature contours obtained for a uniform cold fluid stream flow rate of 0.067 kg/s and hot fluid stream flow rates of 0.033 and 0.05 kg/s for FPHE. The increment in the U-value of DPHE (compared to FPHE) can be evidenced by the simulation results obtained for cold and hot channels of DPHE as given in Fig. 18. While comparing Figs. 12(a), (b), and (c) a high heat transfer coefficient was obtained for a high cold fluid stream flow rate which can be evidenced in Fig. 12(c).

From the temperature contours obtained for both FPHE and DPHE, the outlet temperatures (steady state) of the cold and hot fluid streams were noted and the Nu for the cold fluid was calculated. The results are plotted against Re_h in Fig. 19 for both FPHE and DPHE at three different cold fluid mass flow rates. From Fig. 19, it can be observed that as Re_h increases, Nu_c increases for both FPHE and DPHE. Nu_c increases from 1.9 to 8.7 for DPHE when the hot fluid stream flow rate increases from 0.016 to 0.067 kg/s.

The average percentage increase in the Nu_c of DPHE compared to FPHE was found to be 17.4%, 25.2%, and 41.4% at 0.033 kg/s, 0.05 kg/s and 0.067 kg/s (cold fluid flow rates), respectively. This increment in the Nu_c was because of the increase in the secondary flows generated by the dimples which eventually increases the turbulence of the fluid. At the same time, the secondary vortices of the fluid cause the boundary layer to become thinner, thereby augmenting heat transfer. *Afanasyev et al.* [27] studied the turbulent flow friction and heat transfer behavior of spherical cavities in FPHE. A heat transfer augmentation similar to the present study was noted. It was inferred that the augmentation was due to a complex vortex motion of fluids originating from the spherical cavities.

Won and *Ligrani* [28] also observed a similar heat transfer augmentation by producing multiple pairs of vortices causing secondary advection and turbulence, as fluid flows from upstream to downstream along the dimple. *Moon*, *O'Connell*, and *Sharma* [29] studied heat

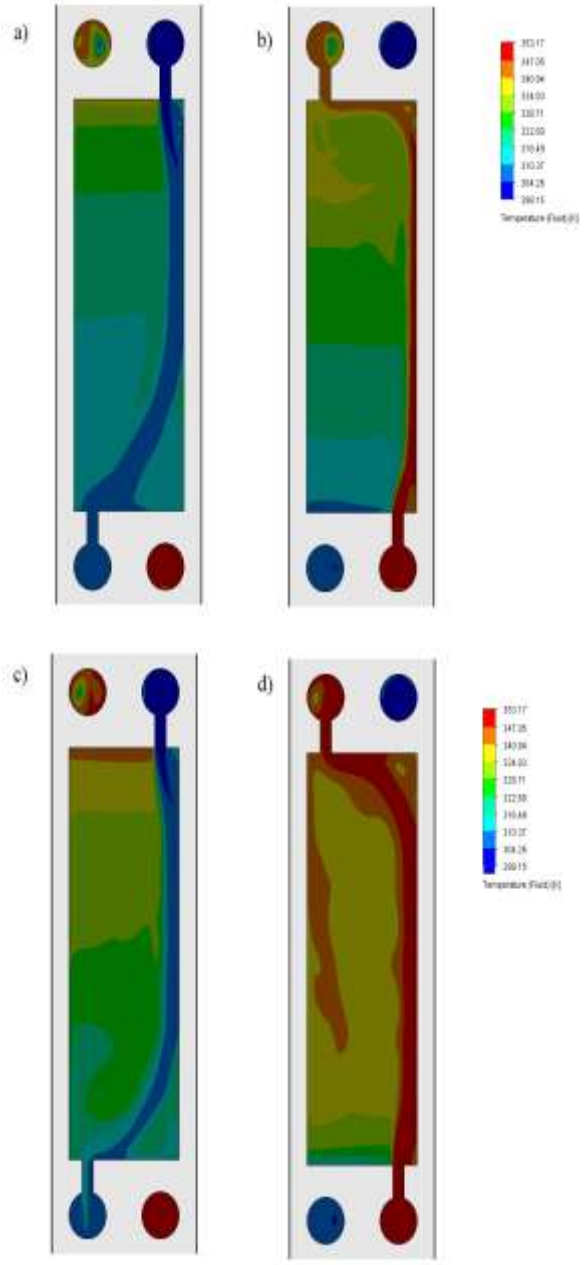

Fig. 13: Temperature contour for FPHE with constant cold fluid flow rate 0.033 kg/s(a) cold channel and (b) hot channel for hot fluid flow rate 0.016 kg/s(c) cold channel and (d) hot channel for hot fluid flow rate 0.05 kg/s.

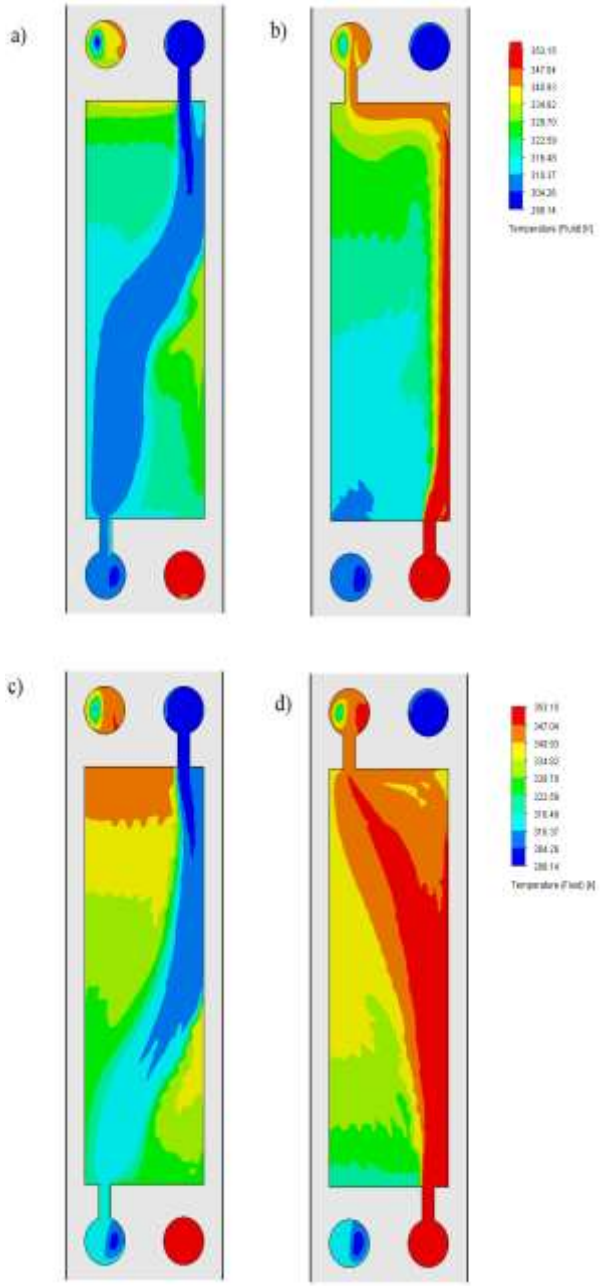

Fig. 14: Temperature contour for DPHE with constant cold fluid flow rate 0.033 kg/s (a) cold channel and (b) hot channel for hot fluid flow rate 0.016 kg/s (c) cold channel and (d) hot channel for hot fluid flow rate 0.05 kg/s.

transfer with a convex-patterned surface and also observed similar results. The obtained results were due to an unsteady state and a vortex-like flow at lower Re, whereas at higher Re, the flow became more turbulent which eventually resulted in heat transfer augmentation. When the flow rate of hot and cold fluid streams increases, the Re of the corresponding fluid increases; this enhances convection arising out of the destruction of the thermal boundary layer by the disturbances in the dimples. This can be well perceived from the temperature contours of the present analysis at various simulation conditions.

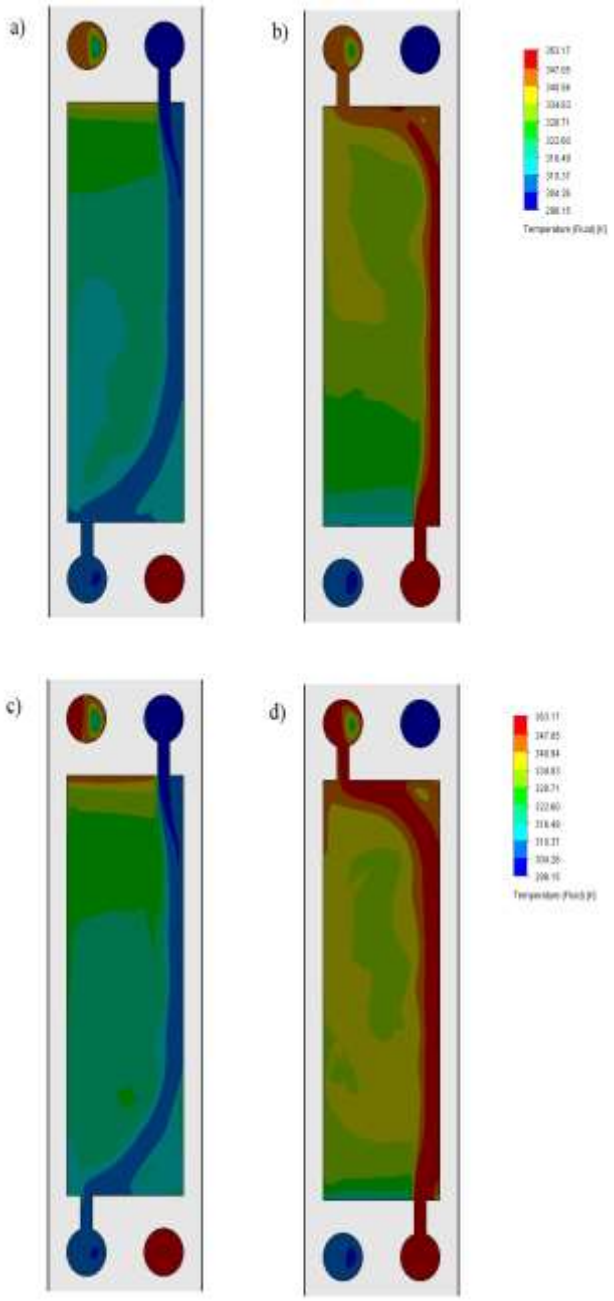

Fig. 15: Temperature contour for FPHE with constant cold fluid flow rate 0.05 kg/s (a) cold channel and (b) hot channel for hot fluid flow rate 0.033 kg/s(c) cold channel and (d) hot channel for hot fluid flow rate 0.067 kg/s.

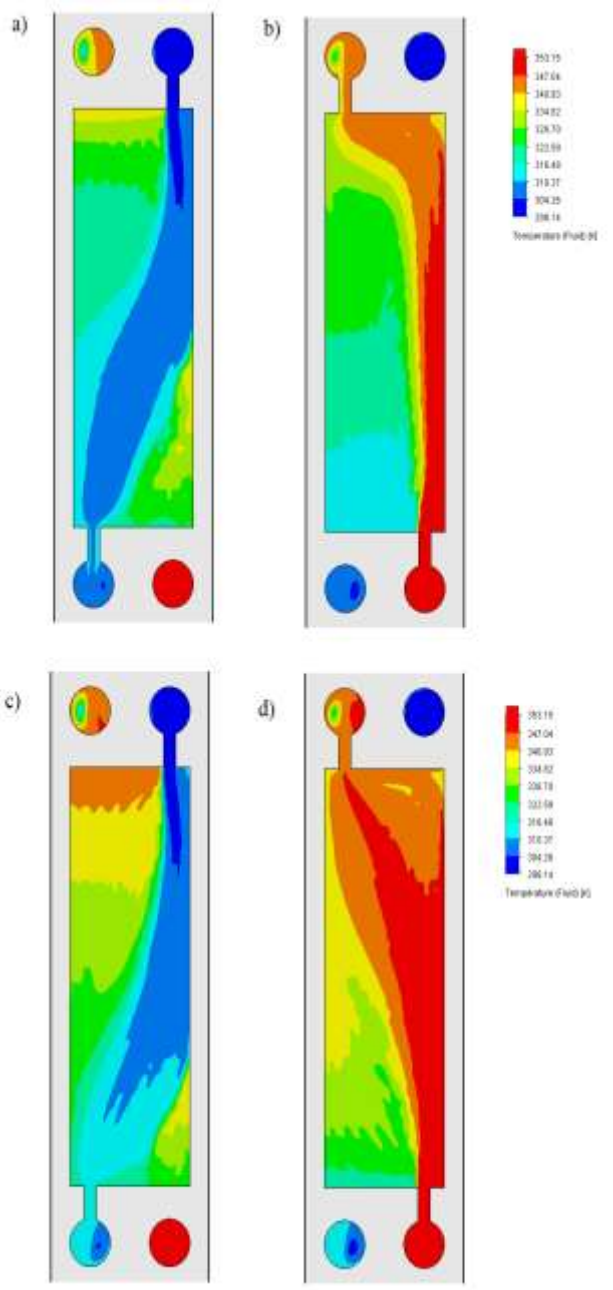

Fig. 16: Temperature contour for DPHE with constant cold fluid flow rate 0.05 kg/s (a) cold channel and (b) hot channel for hot fluid flow rate 0.033 kg/s (c) cold channel and (d) hot channel for hot fluid flow rate 0.067 kg/s.

CONCLUSIONS

The same and different flow analyses using water as working fluids (hot and cold) were numerically studied using the SOLID WORKS 2018 version. The simulation results of DPHE were validated with actual experimental results. The influence of the Reynolds number of the hot fluid on the overall heat transfer coefficient and the Nusselt number of the cold fluid was studied. From the studies, it can be observed that both the heat transfer coefficient and Nusselt number increase with respect to the Reynolds number of the fluid. A correlation was established for the same flow analysis behavior of the FPHE to predict

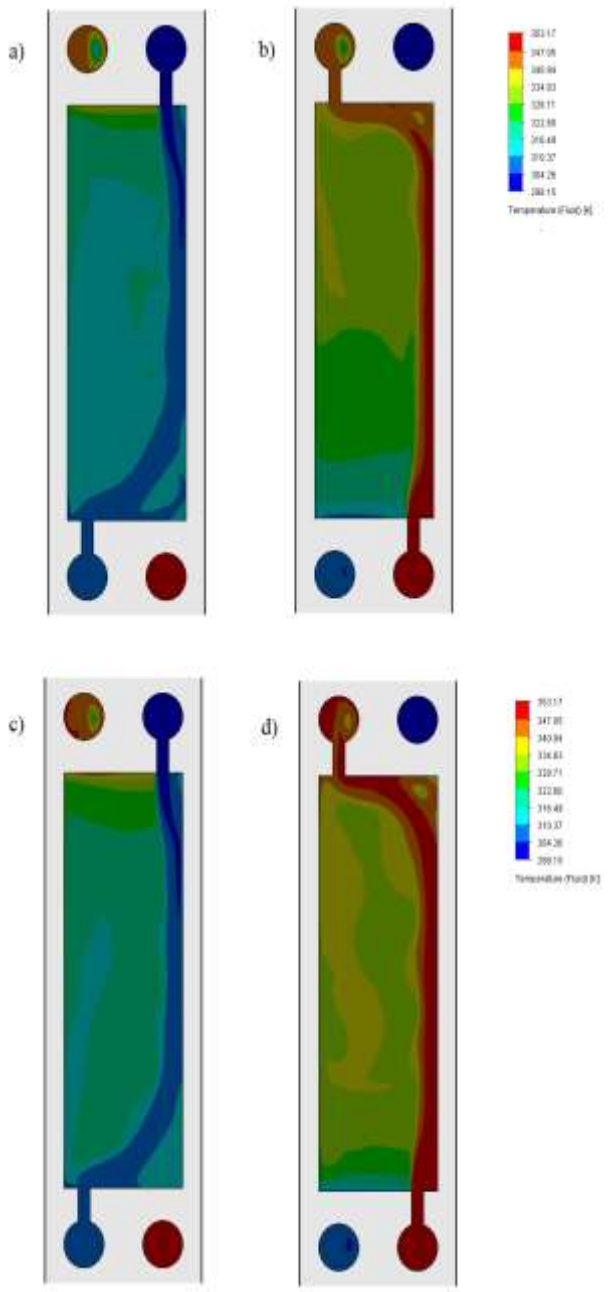

Fig. 17: Temperature contour for FPHE with constant cold fluid flow rate 0.067 kg/s (a) cold channel and (b) hot channel for hot fluid flow rate 0.033 kg/s (c) cold channel and (d) hot channel for hot fluid flow rate 0.05 kg/s.

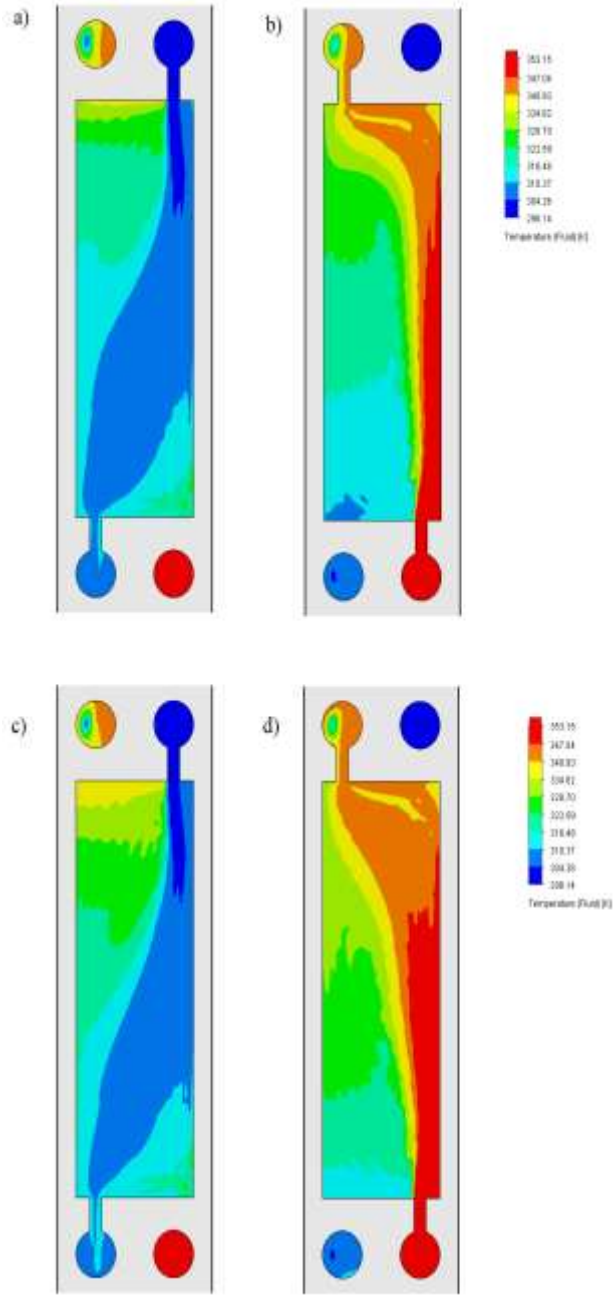

Fig. 18: Temperature contour for DPHE with constant cold fluid flow rate 0.067 kg/s (a) cold channel and (b) hot channel for hot fluid flow rate 0.033 kg/s (c) cold channel and (d) hot channel for hot fluid flow rate 0.05 kg/s.

The Nusselt number. Additionally, the performance of FPHE was compared with DPHE using numerical studies. From the results of the same flow analysis, it can be concluded that the Nusselt number of DPHE is 39% higher than that of FPHE at the highest flow rate of 0.067 kg/s. In different flow analyses, a 41% higher Nusselt number was obtained for DPHE than that for FPHE at the highest mass flow rate of 0.067 kg/s.

Nomenclature

CFD	Computational fluid dynamics
DPHE	Dimple plate Heat Exchanger

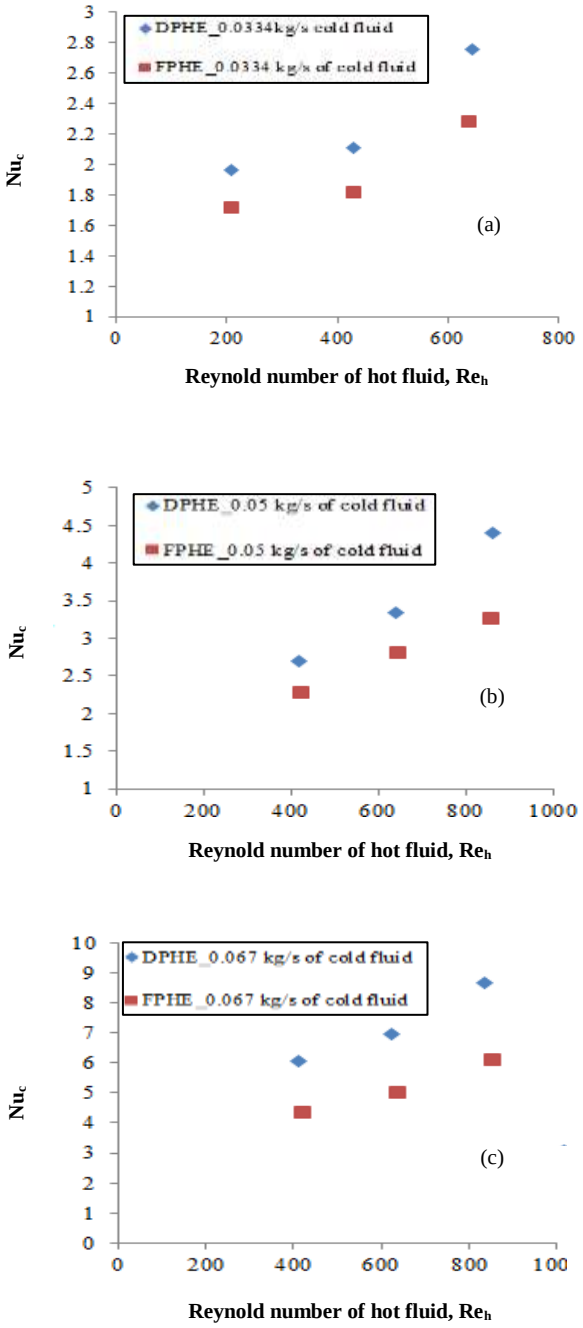

Fig. 19: Effect of Re_h on Nu_c for different flow analyses.

FPHE	Flat plate Heat Exchanger
HE	Heat Exchanger
m_c	Mass flow rate of cold fluid, kg/s
m_h	Mass flow rate of hot fluid, kg/s
Nu	Nusselt number, dimensionless
Nu_c	Nusselt number of cold fluids, dimensionless
PHE	Plate Heat Exchanger
Pr	Prandtl number, dimensionless
Re	Reynolds number, dimensionless
Re_h	Reynolds number of the hot fluid, dimensionless
U	Overall heat transfer coefficient, W/(m^2.K)

Received : Aug. 24, 2021 ; Accepted : Nov. 15, 2021

REFERENCES

[1] Versteeg H.K., Malalasekera W., An Introduction to Computational Fluid Dynamics (1995).

[2] Luki A.A., Ganesan M., Flow Analysis and Characteristics Comparison of Double Pipe Heat Exchanger Using Enhanced Tubes, *IOSR J. Mech. Civ. Eng.*, **7**: 16–21 (2014).

[3] Saleh M.A., Abdel-Hameed H.E., Flow and Heat Transfer Performance of a Dimpled-Inter Surface Heat Exchanger-an Experimental/Numerical Study, *Appl. Therm. Eng.*, **21**: (2002).

[4] Oluyale J.O., Omolayo P.M., Ayoade A.A., Adedayo I.F., Experimental Investigation of Flow and Heat Transfer in a Channel with Dimpled Plate, *J. Phys. Conf. Ser.*, **1378:** 1–13 (2019).

[5] Zhang L., Xiong W., Zheng J., Liang Z., S. Xie S., Numerical Analysis of Heat Transfer Enhancement and Flow Characteristics Inside Cross-Combined Ellipsoidal Dimple Tubes, *Case Stud. Therm. Eng.*, **25:** 1–12 (2021).

[6] Lotfi B., Sundén B., Thermo-Hydraulic Performance Enhancement of Finned Elliptical Tube Heat Exchangers by Utilizing Innovative Dimple Turbulators, *Heat Transf. Eng.*, **41:** 1117–1142 (2020).

[7] Firoozi A., Majidi S., Ameri M., A Numerical Assessment on Heat Transfer and Flow Characteristics of Nanofluid in Tubes Enhanced With a Variety of Dimple Configurations, *Therm. Sci. Eng. Prog.*, **19:** 1–18 (2020).

[8] Sabir R., Khan M.M., Sheikh N.A., Ul-Ahad I., Brabazon D., Assessment of Thermo-Hydraulic Performance of Inward Dimpled Tubes with Variation in Angular Orientations, *Appl. Therm. Eng.*, **170:**

[9] Babu J.S., Sellamuthu P., Analysis of Heat Transfer and Fluid Flow Characteristics of Concentric Tube Heat Exchanger with Dimpled Tube, *J. Xi'an Univ. Agric. Technol.*, **12:** 508–516 (2020).

[10] Piper M., Zibart A., Djakow E., Springer R., Homberg W., Kenig E.Y., Heat Transfer Enhancement in Pillow-Plate Heat Exchangers with Dimpled Surfaces: A Numerical Study, *Appl. Therm. Eng.*, **153:** 142–146 (2019).

[11] Yoon H.S., Park S.H., Choi C., Ha M.Y., Numerical Study on Characteristics of Flow and Heat Transfer in a Cooling Passage with a Tear-Drop Dimple Surface, *Int. J. Therm. Sci.*, **89**: 121–135 (2015).

[12] Shokouhmand H., Esmaeili M.A., Vahidkhah K., Numerical Simulation of Conjugated Heat Transfer Characteristics of Laminar Air Flows in Parallel-Plate Dimpled Channels, *Int. J. Mech. Mechatronics. Eng.*, **5**: 7–14 (2011).

[13] Ligrani P.M., Mahmood G.I., Harrison J.L., Clayton C.M., Nelson D.L., Flow Structure and Local Nusselt Number Variations in a Channel with Dimples and Protrusions on Opposite Walls, *Int. J. Heat Mass Transf.*, **44**: 4413–4425 (2001).

[14] Chimres N., Wang C., Wongwises S., Optimal Design of the Sermi-Dimple Vortex Generator in the Fin and Tube Heat Exchanger, *Int. J. Heat Mass Transf.*, **120**: 1173-1186 (2018).

[15] Vorayos N., Katkhaw N., Kiatsiriroat T., Nuntaphan A., Heat Transfer Behavior of Flat Plate Having Spherical Dimpled Surfaces, *Case Stud. Therm. Eng.*, **8**: 370–377 (2016).

[16] Patel I.H., Borse S.L., Experimental Investigation of Heat Transfer Enhancement over the Dimpled Surface, *Int. J. Eng. Sci. Technol.*, **4**: 3666–3672 (2012).

[17] Katkhaw N., Vorayos N., Kiatsiriroat T., Khunatorn Y., Bunturat D., Nuntaphan A., Heat Transfer Behavior of Flat Plate Having 45^0 Ellipsoidal Dimpled Surfaces, *Case Stud. Therm. Eng.*, **2**: 67–74 (2014).

[18] Elyyan M.A., Rozati A., Tafti D.K., Investigation of Dimpled Fins for Heat Transfer Enhancement in Compact Heat Exchangers, *Int. J. Heat Mass Transf.*, **51**: 2950–2966 (2008).

[19] Abraham J., Maki, R., Hydrodynamics of Laminar Flow Through Dimpled Pipes, *MOJ Civ. Eng.*, **4**: 150–154 (2018).

[20] Pisal, H.C., Ranaware, A.A.: Heat Transfer Enhancement by Using Dimpled Surface, *IOSR J. Mech. Civ. Eng.*, **6**: 7–15 (2013).

[21] Nascimento I.P., Garcia E.C., Heat Transfer Performance Enhancement in Compact Heat Exchangers by Using Shallow Square Dimples in Flat Tubes, *Appl. Therm. Eng.*, **96**: 659–670 (2016).

[22] Shin S., Lee K.S., Park S.D., Kwak J.S., Measurement of the Heat Transfer Coefficient in the Dimpled Channel: Effects of Dimple Arrangement and Channel Height, *J. Mech. Sci. Technol.*, **23**: 624–630 (2009).

[23] Sobachkin A., Dumnov G., Numerical Basis of CAD-Embedded CFD, *In NAFEMS World Congress*, 9-12 (2013).

[24] Soman D.P., Karthika S., Kalaichelvi P., Radhakrishnan T.K., Experimental Study of Turbulent Forced Convection Heat Transfer and Friction Factor in Dimpled Plate Heat Exchanger, *Appl. Therm. Eng.*, **162**: 114254 (2019).

[25] Mahmood G.I., Hill M.L., Nelson D.L., Ligrani P.M., Moon H.K., Glezer B., Local Heat Transfer and Flow Structure on and Above a Dimpled Surface in a Channel, *J. Turbomach.*, **123**: 115–123 (2001).

[26] Ahmed H., Qureshi S.R., Qureshi N., CFD and Heat Transfer Analysis on Dimpled Plate Heat Exchangers

[27] Afanasyev V.N., Chudnovsky Y.P., Leontiev A.I., Roganov P.S., Turbulent Flow Friction and Heat Transfer Characteristics For Spherical Cavities on a Flat Plate, *Exp. Therm. Fluid Sci.*, **7:** 1–8 (1993).

[28] Won S.Y., Ligrani P.M., Flow Characteristics Along and Above Dimpled Surfaces with Three Different Dimple Depths within A Channel, *J. Mech. Sci. Technol.*, **21:** 1901–1909 (2007).

[29] Moon H.K., O'Connell T., Sharma R., Heat Transfer Enhancement Using a Convex-Patterned Surface, *J. Turbomach.*, **125**: 274–280 (2003).